Hindawi Publishing Corporation
Advances in Chemistry
Volume 2016, Article ID 6848693, 14 pages
http://dx.doi.org/10.1155/2016/6848693

Research Article

Zirconium-Doped Fungal Sorbents: Preparation, Characterization, Adsorption Isotherm, and Kinetic and Mathematical Modelling Study for Removal of Fluoride

Poornima G. Hiremath and Thomas Theodore

Department of Chemical Engineering, Siddaganga Institute of Technology, Tumkur, Karnataka 572103, India

Correspondence should be addressed to Thomas Theodore; theodorethomas2015@gmail.com

Received 26 April 2016; Accepted 13 June 2016

Academic Editor: Peiqiang Li

The present study involves usage of more efficient and eco-friendly zirconium-doped, fluoride-resistant fungal biosorbents for removal of excess fluoride from groundwater. It was observed that >94% fluoride removal was possible at optimal conditions for the four fungal species studied. The adsorption isotherm studies indicated that zirconium-doped *Aspergillus ficuum* SIT-CH-2, *Aspergillus terreus* SIT-CH-3, and *Aspergillus flavipes* SIT-CH-4 were best described by Freundlich isotherm and zirconium-doped *Penicillium camemberti* SIT-CH-1 fitted well with Langmuir adsorption isotherm equation. The pseudo-second-order kinetics model showed the best fit for all of the four zirconium-doped fungal species for the fluoride biosorption.

1. Introduction

Fluoride is the ionic form of the element fluorine belonging to halogen group. Fluoride exists due to both natural and anthropogenic causes in the environment. The natural cause for the presence of fluoride ions in groundwater is due to fluoride leaching from rocks or soil into theunderground bed, whereas the anthropogenic reason is the wide use of fluorinated compounds by industry [1]. The concentration of fluoride ion in drinking water will determine whether it is useful or hazardous to human health. Fluoride ingestion up to 0.6 ppm (as per the WHO) is required for bone and teeth development. The WHO standards and BIS: 10500 (1983) have set 1.5 ppm as a safe limit of fluoride in drinking water for human consumption [2, 3]. Fluoride intake beyond this limit causes dental and skeletal fluorosis and nonskeletal manifestations. All over the world many countries including India, USA, Pakistan, South African countries, Bangladesh, Morocco, Argentina, Middle East countries, and New Zealand are suffering from excess fluoride in groundwater [4]. It is estimated that more than 70 million people around the world suffer from fluorosis due to chronic exposure to high levels of fluoride in drinking water [5]. Several districts in India are affected by high fluoride water, which include Andhra Pradesh, Tamil Nadu, Uttar Pradesh, Gujarat, Rajasthan, Haryana, Bihar, and Karnataka [4, 6]. Around 4.6% of geological area of Karnataka has high fluoride concentration, which includes Tumkur, Gulbarga, Bellary, and Raichur [4]. Different methods like coagulation and precipitation and oxide minerals, ion exchange, and adsorption have been tried for removing excess fluoride from water. While chemical precipitation produces toxic sludge, the ion-exchange method is expensive due to costly ion-exchange resins [7]. Hence, alternative bio-based methods of fluoride removal and recovery have to be considered [8]. Fungi can be of low cost as they are available as industrial waste products. Fungi are generally used for the production of citric acid and many enzymes. It has been proven earlier that physicochemical modifications of fungal biomass could lead to better sorption uptakes, better adsorption, or higher mechanical stability. Thus, fungi, which are known to possess good heavy metal sorption capacity [8], are bonded with tetravalent zirconium and used as an adsorbent for fluoride removal. The primary aim of the present study was to

Table 1: GenBank accession number of the fungal species.

Species name	Accession number
Penicillium camemberti SIT-CH-1	KT200225
Aspergillus terreus SIT-CH-3	KT200226
Aspergillus ficuum SIT-CH-2	KT200227
Aspergillus flavipes SIT-CH-4	KT364632

determine the possibilities for usage of zirconium-doped fungal biomass in biosorption of fluoride. The next objective was to assess the optimum conditions of fluoride sorption from aqueous solutions.

2. Experimental

2.1. Pretreatment of Fungal Biosorbents. The four fungal species isolated from soil samples collected from fluoride affected areas and identified as *Penicillium camemberti* SIT-CH-1, *Aspergillus ficuum* SIT-CH-2, *Aspergillus terreus* SIT-CH-3, and *Aspergillus flavipes* SIT-CH-4 were used for defluoridation studies. The accession numbers of the same are listed in Table 1. The fungal species were cultured in potato dextrose broth and the obtained biomass was autoclaved. The fungal mats were separated, washed with distilled water, and dried in a hot-air oven at 70°C for 24 h. The dried biomass was then pulverized to a fine powder for better absorption of zirconium. The powdered fungi were then doped with zirconium by adding 5% $ZrOCl_2{\cdot}10H_2O$ solution to the fungal powder in the ratio of 3 : 1. This ratio was fixed based on the optimum removal efficiency of adsorbent. The mixture was then equilibrated for 72 h at 25°C. The zirconium-doped fungi were then filtered, washed with water to remove free zirconium, dried in an oven at 100°C, and later used to investigate the defluoridation capacity [9].

2.2. Fluoride Estimation. Fluoride was estimated by the Mettler Toledo fluoride ion selective electrode (perfectION™ combined fluoride electrode make) and Mettler Toledo ion analyzer (SevenCompact pH/ion meter S220 make). Total ionic strength adjusting buffer-III (TISAB-III) solution was added to the samples in the ratio of 1 : 10 to regulate the ionic strength of samples and standard solutions. TISAB-III maintained the solution pH between 5 and 5.5, separated loosely bound fluoride ions, and eliminated the interference effect of complexing ions. One litre of 100 ppm NaF solution was prepared which was subsequently diluted to form 10, 20, 30, and 40 ppm solutions. These solutions were employed to calibrate the abovementioned instrument.

2.3. Batch Sorption Experiments. Stock solutions of fluoride were prepared by dissolving sodium fluoride in known amount of distilled water. The initial pH of the solution was adjusted to a predetermined value using HCl or NaOH. The experiments were carried out in 250 mL polypropylene containers with known mass of biosorbent added to the feed solution. The containers were shaken at 190 rpm using rotary shaker incubator for a known period of time at 30°C. The solution was separated from the biomass using Whatman filter paper number 42. The solution was analyzed for the residual fluoride concentration by the fluoride ion selective electrode.

The percentage biosorption was calculated using

$$\%\ \text{biosorption} = \frac{(C_0 - C_e)}{C_0} * 100. \tag{1}$$

The amount of fluoride (in mg) adsorbed per g of adsorbent after equilibrium (q_e) was calculated using

$$q_e = \frac{(C_0 - C_e)\,V}{M}, \tag{2}$$

where C_0 and C_e (ppm) represent the initial and equilibrium fluoride concentrations in the solution, respectively. V is the volume of the solution (L) and M is the mass of adsorbent (g).

2.4. Optimization of Biosorption Process. In this study, the four main parameters including initial fluoride concentration (10–100 mg/L), pH (2–8), biosorbent dose (0.1–1 g/100 mL), and contact time (30–240 min) were optimized using central composite design (CCD) of response surface methodology (RSM) to obtain the optimal conditions for maximum fluoride removal [10]. RSM helps in finding out the optimum conditions of the process. Design Expert software 9.0.3.1 (Stat-Ease, MA) was employed for optimizing the biosorption process and also to understand the main and interaction effects of each process variable. For selecting the levels of different process parameters, primarily batch biosorption studies were carried out. The design composed of a total of 30 runs with six replicates and the alpha value was considered as 1 by selecting the face-centered option. The design with three levels, low, medium, and high, was coded as −1, 0, and +1, respectively. The experimental design matrix obtained by CCD design was used to perform the related experiments. The adequacy and testing hypotheses on the parameters were corroborated by ANOVA.

The polynomial equation model used for predicting the optimal conditions was represented by

$$Y = \beta_0 + \sum_{i}^{k} \beta_i x_i + \sum_{ii}^{k} \beta_{ii} x_i^2 + \sum_{i<j} \beta_{ij} x_i x_j, \tag{3}$$

where Y is the response, x_i, x_j are the independent variables, and β_0, β_i, β_{ii}, β_{ij} are the regression coefficients.

2.4.1. Desirability Function. Desirability function, D, is a statistical tool used for optimization of process variables. The desirability value lies between zero and one, zero being the least desirable and one being the most desirable. The desirability function is adjusted to maximum to obtain the optimum values [11].

2.5. Adsorption Isotherms. Adsorption isotherm graphically represents the relation between the solute adsorbed onto a unit mass of adsorbent and the residual solute present in the

solution at equilibrium conditions. In the present study, the Freundlich, Langmuir, Dubinin-Radushkevich (D-R), and Temkin adsorption isotherm models were used for analyzing the equilibrium data. The isotherm constants indicated the biosorbents capability for defluoridation.

The Langmuir adsorption isotherm model is given by [12]

$$q_e = \frac{q_m K_a C_e}{1 + K_a C_e}, \tag{4}$$

where C_e is the equilibrium concentration (ppm), q_e represents the adsorbent uptake capacity at equilibrium concentration, q_m is the adsorbent uptake capacity to form a monolayer (mg/g), and K_a is the Langmuir constant. This model is applicable for monolayer adsorption with a fixed quantity of identical sites. The K_a and q_m values were calculated from the slope and the intercept of the plot $1/q_e$ versus $1/C_e$. The values of the Langmuir separation factor, R_L obtained from (5), indicate whether the adsorption is either unfavorable when $R_L > 1$, linear when $R_L = 1$, favorable when $0 < R_L < 1$, or irreversible if $R_L = 0$. Consider the following:

$$R_L = \frac{1}{1 + K_a C_o}. \tag{5}$$

The Freundlich model, which is indicative of surface heterogeneity of the sorbent, is given by [12]

$$q_e = K_f C e^{(1/n)}, \tag{6}$$

where K_f and $1/n$ are Freundlich constants related to adsorption capacity and adsorption intensity, respectively.

D-R isotherm is generally applied to express the adsorption mechanism with a quasi-Gaussian distribution with broadening at high adsorption energies [13]. The model has often successfully fitted high solute activities and the intermediate range of concentration data well. The approach was usually applied to distinguish the physical and chemical adsorption of metal ions with its mean free energy; E per molecule of adsorbate (for removing a molecule from its location in the sorption space to infinity) can be computed by [12]

$$\begin{aligned} \ln q_e &= \ln q_m - \beta\varepsilon^2, \\ \varepsilon &= RT \ln\left[1 + \frac{1}{C_e}\right], \end{aligned} \tag{7}$$

where q_e is the number of fluoride ions adsorbed per unit weight of adsorbent (mol/g), q_m is the theoretical isotherm saturation capacity (mol/g), β is the D-R isotherm constant (mol^2/kJ^2), ε is the D-R isotherm constant, R is the gas constant (8.314 J/mol K), T is the absolute temperature (K), and C_e is the adsorbate equilibrium concentration (mg/L). The slope of the plot of $\ln q_e$ versus ε^2 gives β (mol^2/kJ^2) and the intercept yields the sorption capacity, q_m (mol/g). To evaluate the nature of interaction between fluoride ions and the binding sites, the mean free energy of sorption per mole of the adsorbate, which is the energy required to transfer one mole of an adsorbate to the surface from infinity in solution, was determined as follows [12]:

$$E = \frac{1}{\sqrt{-2\beta}}. \tag{8}$$

The Temkin isotherm contains a factor that explicitly takes into account the adsorbent-adsorbate interactions. By ignoring the extremely low and large value of concentrations, the model assumes that the heat of adsorption (function of temperature) of all molecules in the layer would decrease linearly rather than logarithmically with coverage.

As implied in the equation, its derivation is characterized by a uniform distribution of binding energies (up to some maximum binding energy). It was carried out by plotting the quantity sorbed q_e against $\ln C_e$ and the constants were determined from the slope and intercept [12].

The model is represented by

$$q_e = B \ln\left(A_T C_e\right), \tag{9}$$

where A_T represents Temkin isotherm equilibrium binding constant (L/g), b is the Temkin isotherm constant, R is the universal gas constant (8.314 J/mol/K), T is the temperature, and $B = RT/b$ = constant related to heat of sorption (J/mol). By plotting q_e versus $\ln C_e$ (see (9)), the constants A_T and B are determined.

2.6. Kinetics of Sorption. The studies of adsorption equilibrium are important in determining the effectiveness of adsorption; however, it is also necessary to identify the types of adsorption mechanism in a given system. In this study, four different models (first-order, pseudo-second-order, Elovich, and intraparticle diffusion) were used to predict the adsorption kinetics of fluoride on zirconium-doped fungal biosorbents. In order to obtain the data of concentration of fluoride versus time, samples of solution were withdrawn at regular intervals of time (10, 20, 30, 60, 120, 180, 240, and 300 min) during biosorption and analyzed for fluoride after separation of biomass by filtration.

The first-order rate equation is given by [14]

$$\frac{1}{q_t} = \frac{1}{q_1} + \frac{k_1}{q_1 t}, \tag{10}$$

where q_t is the amount of adsorbed fluoride per unit weight of biosorbent, mg/g; t is the time, min; q_1 is the amount of fluoride adsorbed per unit weight of biosorbent at equilibrium, mg/g; and k_1 is the first-order rate constant, min^{-1}. A straight line of $1/q_t$ versus $1/t$ suggests the applicability of this kinetic model. q_1 and k_1 were determined from the intercept and slope of the plot.

In addition, the experimental data was also applied to the following pseudo-second-order kinetic model equation [12]:

$$\frac{t}{q_t} = \frac{1}{k_2 q_2^2} + \frac{t}{q_2}, \tag{11}$$

where q_2 is the maximum sorption capacity, mg/g; q_t is the amount of fluoride adsorbed at equilibrium, mg/g; t is

the contact time, min; and k_2 is the pseudo-second-order chemisorption (g/mg·min). q_2 and k_2 values were obtained from the intercept and slope of the plot of t/q_t versus t.

To understand the mechanism of the fluoride adsorption onto zirconium-doped fungal biomass, intraparticle diffusion-based mechanism was studied. The intraparticle diffusion equation can be described as [12]

$$q_t = k_i t^{1/2} + C, \tag{12}$$

where k_i is the intraparticle diffusion rate constant (mg/g min).

The Elovich model assumes that the adsorbent surface is energetically heterogeneous and can also describe the chemisorption process [15]. The linearized equation is given by

$$q_t = \beta \ln(\alpha\beta) + \beta \ln t, \tag{13}$$

where α = sorption rate (mmol/(g min)) and β = desorption constant (g/mmol).

2.7. Characterization of Sorbents. The biosorbents were examined using SEM-EDS. The SEM-EDS analyses were carried out with the help of a computer-controlled FESEM with EDS detector. SEM images enable a direct observation of changes in the surface morphology and EDS qualitatively determines the elements present on the biosorbent before and after adsorption.

Fourier Transform Infrared (FTIR) spectra of biosorbents before and after adsorption were recorded. FTIR analyses of fungal biosorbents were carried out at room temperature on Spectrum Two™ from PerkinElmer, USA, at a resolution of 2 cm^{-1} in the wave number range 4000–400 cm^{-1} for studying the chemical groups on the surface of the zirconium-treated fungal powder. A small amount of sample (0.2 g) was thoroughly mixed with ground KBr in an agate mortar and a disc was prepared in vacuum while maintaining a pressure of 33 kg/cm^2.

The XPS spectra were measured on a Kratos Axis Ultra spectrometer (UK). An Al Kα anode radiation source was used as the excitation source. The XPS results were corrected by using C1s calibration energy of 284.6 eV. XPS data processing and peak fitting were performed using a nonlinear least-squares fitting program (XPSPeak software 4.1, R. W. M. Kwok).

Mastersizer 2000 (Malvern Instruments Inc., UK) was used to determine the particle size of the biosorbent. BET surface area was analyzed using TriStar 3000 V6.05 A.

2.7.1. Zeta Potential Measurements. The zeta potential (ζ) was measured according to a previously reported procedure [15] for 10 g/L of biosorbent suspension with 100 ppm of fluoride and without fluoride in the pH range of 2–10 using a Zetasizer 2000 (Malvern Instruments Inc., UK). The 0.01 mol/L $NaNO_3$ was added as the background electrolyte and aged for 24 h at a fixed temperature. The initial pH was adjusted using HNO_3 or NaOH. The samples for analysis were prepared according to the following procedure. Biosorbent suspensions with or without F^- at the desired pH and ionic strength were shaken at 25°C and 180 rpm for 24 h. The equilibrium pH was then measured and the suspension was injected into the electrophoretic cell for zeta potential measurement in triplicate, after which the average reading was recorded. The pH at the point of zero charge (pH_{ZPC}) was obtained by interpolating the zeta potential data to the zero potential [16].

3. Results and Discussion

3.1. Characterization of the Biosorbents. The particle size of zirconium-doped fungal biosorbents and their BET surface area and specific gravity are shown in Tables 2 and 3, respectively.

3.1.1. FTIR Studies. FTIR spectra were obtained to determine the typical functional groups present on zirconium-doped *Penicillium camemberti* SIT-CH-1, *Aspergillus ficuum* SIT-CH-2, *Aspergillus terreus* SIT-CH-3, and *Aspergillus flavipes* SIT-CH-4 species, which are responsible for biosorption of fluoride ions. The fluoride biosorption on the fungal biomass resulted in several changes in peaks such as the shifts and decrease in the percentage of transmittance in the IR spectra of the solid surface in the range 4000–400 cm^{-1} as indicated in Figure 1 and Table 4. The elucidation of the spectra was based on the information acquired from literature [17].

The FTIR spectra confirm the presence of hydroxyl, carboxyl, amine, and phosphate groups on the surface of fungal biomass and may be considered as important sorption sites (Figure 1 and Table 4). The peaks for -N-H shifted slightly in the fluoride-laden biomass. This reduction in wave number may indicate the interaction of $-NH_2$ groups of the biomass with fluoride ions. The hydrogen bonding in amines is weaker than that of hydroxyl groups, so $-NH_2$ stretching bands are not as broad or intense as -OH stretching bands [17]. Slight broadening of $-NH_2$ stretching band in the fluoride biosorbed fungal biomass may be due to hydrogen bonding between the protonated amine ($-NH_3^+$) and fluoride ions [17]. Similar results were reported by other authors while studying fluoride sorption on *Pleurotus eryngii* white-rot fungus [18]. Since Zr-F stretching and F-Zr-F bending vibrations occur around 375–475 cm^{-1} and 240–350 cm^{-1}, respectively, [19] these peaks were not observed in the present study with a mid-range infrared spectrophotometer.

3.1.2. Zeta Potential Studies. The zeta potential of the zirconium-doped fungal biomass in the absence (0 ppm F^-) and presence of fluoride (100 ppm F^-) is depicted in Figure 2. Linear interpolation of the experimental data gave the pH_{zpc} value of the biosorbents between 6 and 7 for all the four biosorbents before fluoride adsorption, that is, at 0 ppm F^- concentration. There was a shift in pH_{zpc} towards a smaller value and the zeta potential gained more negative values over the entire pH range considered when the 100 ppm fluoride solution was added. The shifts in the pH_{zpc} with increasing fluoride concentration confirmed strong specific fluoride ion biosorption and direct chemical bond formation [16]. This

Table 2: Particle size analysis of zirconium-doped fungal biosorbents.

Species	$D(v, 0.1)/\mu m$	$D(v, 0.5)/\mu m$	$D(v, 0.9)/\mu m$
Penicillium camemberti SIT-CH-1	2.842	12.49	104.803
Aspergillus ficuum SIT-CH-2	3.84	19.6	192.71
Aspergillus terreus SIT-CH-3	2.757	15.956	110.309
Aspergillus flavipes SIT-CH-4	3.127	11.157	148.957

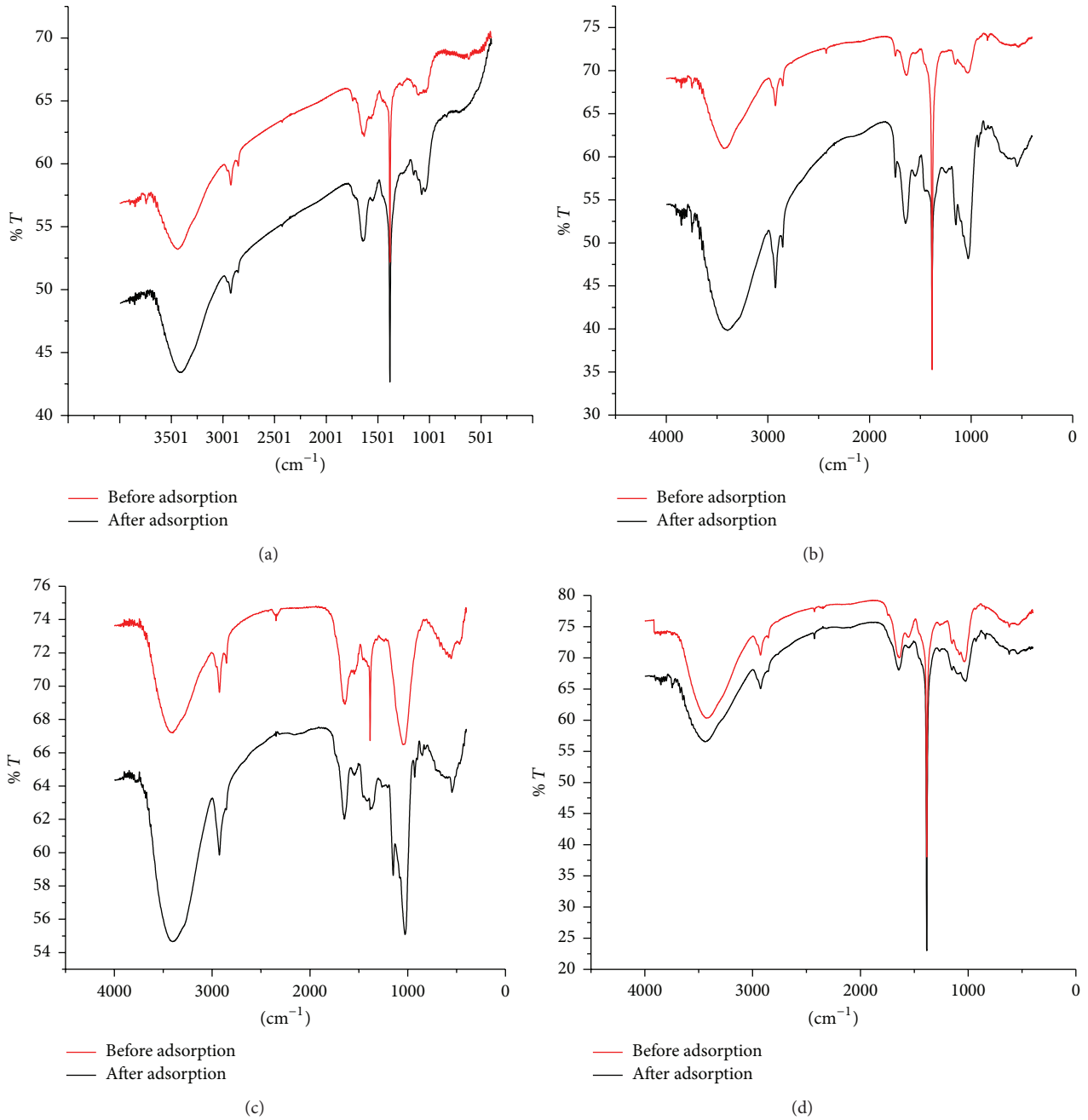

Figure 1: FTIR spectra of zirconium-doped fungal biomass and fluoride treated zirconium-doped (a) *Penicillium camemberti* SIT-CH-1, (b) *Aspergillus ficuum* SIT-CH-2, (c) *Aspergillus terreus* SIT-CH-3, and (d) *Aspergillus flavipes* SIT-CH-4 fungal biomass at pH 2.

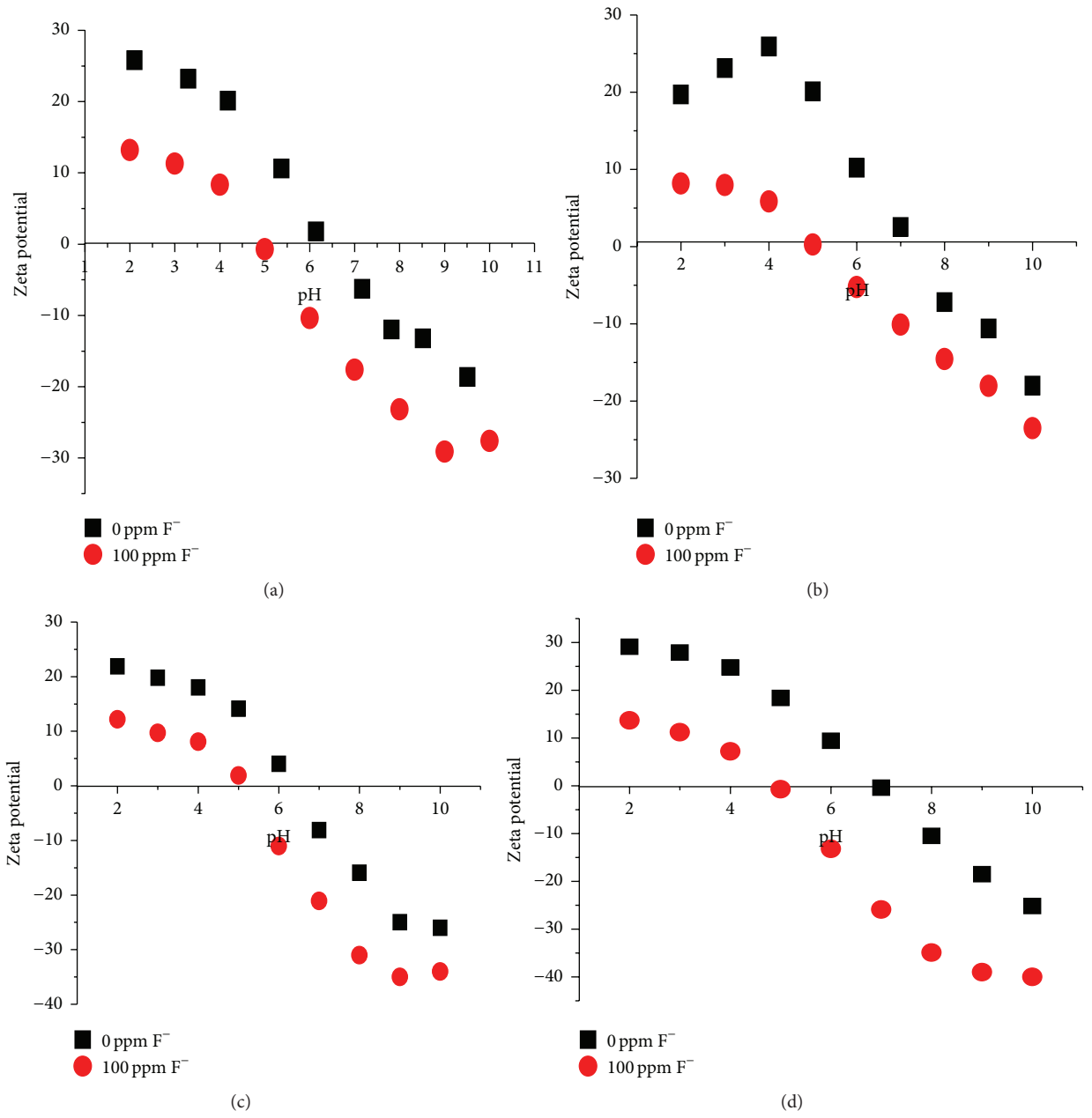

FIGURE 2: Zeta potential values of the zirconium-doped (a) *Penicillium camemberti* SIT-CH-1, (b) *Aspergillus ficuum* SIT-CH-2, (c) *Aspergillus terreus* SIT-CH-3, and (d) *Aspergillus flavipes* SIT-CH-4 fungal biomass before and after fluoride adsorption; adsorbent dose, 10 g/L; temperature, 25°C.

TABLE 3: BET surface area and specific gravity.

Species	BET surface area/m^2/g	Specific gravity
Penicillium camemberti SIT-CH-1	10.63	0.24
Aspergillus ficuum SIT-CH-2	0.30	1.35
Aspergillus terreus SIT-CH-3	10.60	0.73
Aspergillus flavipes SIT-CH-4	2.81	0.39

may be due to the replacement of the surface Zr-OH groups with Zr-F structures. At pH < 7, the surface charge is positive, consistent with protonation of the surface hydroxyl groups. Here, the pH of the fluoride solution becomes lower than zero point charge and creates a higher fluoride affinity via electrostatic attraction, promoting fluoride adsorption. At pH > 7, the surface charge is negative due to surface hydroxyl group deprotonation, which repulses fluoride ions.

3.1.3. SEM and EDS Studies. Figure 3 shows SEM images for the four zirconium-doped fungal species studied. The surface morphology of biomass, after adsorption, shows few particles of irregular shape adhering to the surface whereas it is missing in the SEM images of biomass before adsorption.

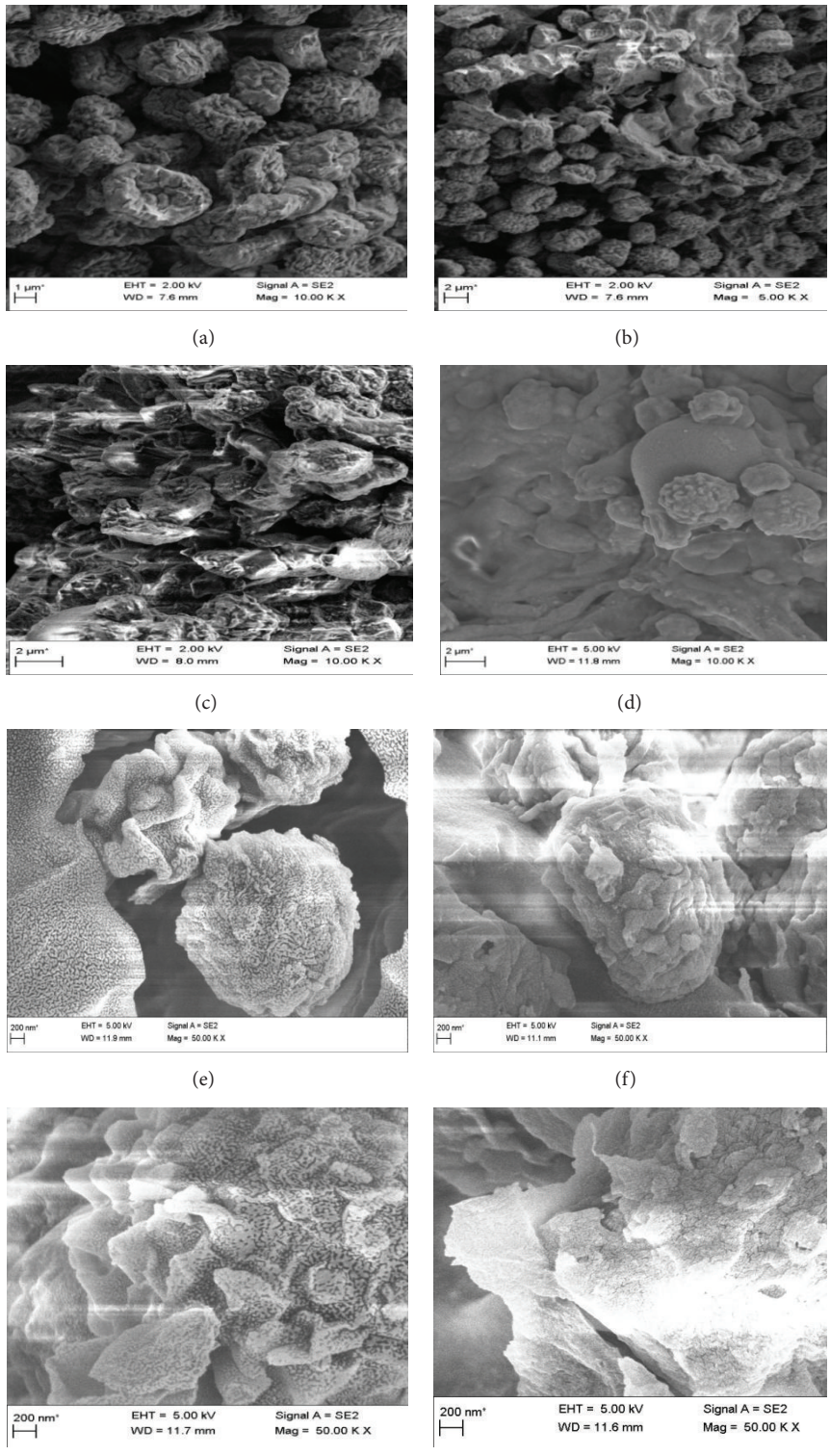

Figure 3: Scanning Electron Microscopy (SEM) images of zirconium-doped fungal biomass: *Penicillium camemberti* SIT-CH-1 (a) before and (b) after adsorption, *Aspergillus ficuum* SIT-CH-2 (c) before and (d) after adsorption, *Aspergillus terreus* SIT-CH-3 (e) before and (f) after adsorption, and *Aspergillus flavipes* SIT-CH-4 (g) before and (h) after adsorption.

Table 4: Surface functional groups observed on the zirconium-doped fungi biomass before and after biosorption.

Before biosorption/cm^{-1}	After biosorption/cm^{-1}	Bands indicating functional groups
Zirconium-doped *Penicillium camemberti* SIT-CH-1		
3437	3412	-NH_2 and -OH stretching
2925	2962	C-H stretching
1634	1634	C=C stretching, H-O-H bending
1385	1385	C-N deformation, Zr-OH bending
1033	1076	C-O deformation, PO_4^{3-} group vibration
Zirconium-doped *Aspergillus ficuum* SIT-CH-2		
3401	3402	-NH_2 and -OH stretching
2926	2926	C-H stretching
1746	1745	C=C stretching
1384	1384	C-N deformation, Zr-OH bending
1029	1035	C-O deformation, PO_4^{3-} group vibration
598	544	C-C skeleton
Zirconium-doped *Aspergillus terreus* SIT-CH-3		
3413	3406	-NH_2 and -OH stretching
2925	2926	C-H stretching
1640	1646	C=C stretching, H-O-H bending
1384	1384	C-N deformation, Zr-OH bending
1044	1027	C-O stretching, PO_4^{3-} group vibration
556	547	C-C skeleton
Zirconium-doped *Aspergillus flavipes* SIT-CH-4		
3430	3437	-NH_2 and -OH stretching
2926	2926	C-H stretching
1639	1644	C=C stretching, H-O-H bending
1384	1384	C-N deformation, Zr-OH bending
1081	1083	C-O stretching, PO_4^{3-} group vibration
537	541	C-C skeleton

It may be noted here that the distribution of zirconium and in turn fluoride on the fungal biomass was found to be nonuniform during the SEM studies. This may be due to very low concentrations of zirconium on biomass and fluoride in solution.

Elemental composition of biomass before and after adsorption analyzed by EDS is indicated in Figure 4. The percentage chemical composition of zirconium-doped fungal biomass using EDS analysis is represented in Supplementary Information (SI) section in Table S1 in Supplementary Material available online at http://dx.doi.org/10.1155/2016/6848693. In Figure 4 and Table S1, the EDS analysis indicates the presence of C, O, Cl, and Zr before fluoride adsorption, whereas the composition is C, Cl, F, and Zr after fluoride adsorption. Thus, EDS analysis confirms the presence of fluoride on the biomass after adsorption.

3.1.4. XPS Studies. The wide spectra of the zirconium-doped fungal biomass before and after adsorption are displayed in Figure 5. In the inset of Figure 5, the enlarged spectra with zirconium peak at 185 eV are highlighted. Before fluoride adsorption, prominent peaks were located at 185 eV. After fluoride adsorption, the peaks broadened and shifted to a higher binding energy by about 0.3 and 0.5 eV, respectively. These changes must be due to the formation of a bond between zirconium and fluoride. This is as expected when zirconium is subjected to greater electron withdrawal when bound to fluorine. Bonding to fluorine causes the loss of electron density at zirconium, which in turn raises its binding energy [20]. Since zirconium is impregnated on fungal biomass, several peaks are observed in the XPS spectra. This might be due to the several organic components present on the surface of the fungal biomass along with zirconium.

3.2. Adsorption Isotherms. The mechanism of fluoride adsorption from aqueous solutions onto zirconium-doped fungal species is determined using adsorption isotherms and is shown in Table 5 and in Supplementary Information (SI) section in Figure S1. The correlation coefficients for the linear regression fit, the constant values, the slope, and intercept values of each adsorption isotherm are also mentioned in Table 5. It was found from the isotherm studies that the zirconium-doped *Aspergillus ficuum* SIT-CH-2, *Aspergillus terreus* SIT-CH-3, and *Aspergillus flavipes* SIT-CH-4 were best described by Freundlich isotherm. The Langmuir adsorption isotherm best described the equilibrium data for zirconium-doped *Penicillium camemberti* SIT-CH-1 biosorbent. The Langmuir isotherm is linear with

Table 5: Isotherm parameters for the fluoride removal by zirconium-doped fungal biosorbents.

Adsorption isotherm	*Penicillium camemberti* SIT-CH-1 + zirconium	*Aspergillus ficuum* SIT-CH-2 + zirconium	*Aspergillus terreus* SIT-CH-3 + zirconium	*Aspergillus flavipes* SIT-CH-4 + zirconium
Freundlich isotherm				
Slope: $1/n$	1.19	0.399	1.858	1.038
Intercept: $\ln K_f$	−0.45	1.583	−0.45	0.331
n	0.838	2.5	0.538	0.963
K_f	0.635	4.87	0.636	1.393
R^2	0.749	0.97	0.914	0.947
Langmuir isotherm				
Slope: $1/q_m K_a$	0.89	0.1	0.611	0.426
Intercept: $1/q_m$	0.005	0.06	0.036	0.023
q_m (mg g^{-1})	216.83	15.85	27.654	43.58
K_a (L mg^{-1})	0.0052	0.63	0.059	0.054
R_L	0.659	0.015	0.203	0.156
R^2	0.934	0.388	0.778	0.618
D-R isotherm				
Slope: β	$-1.29 * 10^{-05}$	$-1E-06$	$-9.4E-06$	$-4.5E-06$
Intercept: $\ln(q_m)$	3.309	2.92	4.33	3.228
q_m (mg g^{-1})	27.375	18.54	76.35	25.23
E (kJ mol^{-1})	196.52	704.09	230.15	332.41
R^2	0.45	0.517	0.822	0.302
Temkin isotherm				
Slope: $(B = RT/b)$ (J/mol)	28.743	4.79	65.07	25.62
Intercept: $B \ln A_T$	−58.149	1.27	−97.8	−40.12
b (dimensionless)	87.64	524.91	38.71	98.32
A_T (L g^{-1})	0.132	1.303	0.222	0.208
R^2	0.505	0.475	0.827	0.555

concentration and surface saturation is reached at higher concentrations. This better fit of equilibrium data to the Langmuir isotherm suggests monolayer coverage of fluoride onto the zirconium-doped fungal *Penicillium camemberti* SIT-CH-1 [15]. The constants "K_a" express the affinity between the adsorbent and adsorbate. The Langmuir isotherm parameter q_m, which is a measure of the monolayer capacity of the adsorbent, and the Freundlich isotherm parameter K_f, which indicates the extent of adsorption, follow the same trend and were good measures of the biosorption capacity of the different zirconium-doped fungal biosorbent samples. A high value of the adsorption parameter "n" in the Freundlich isotherm indicates a strong bond between the adsorbent and the adsorbate, a desired characteristic in adsorption processes [15].

3.3. Adsorption Kinetics. Adsorption kinetic parameters for the adsorption of fluoride by zirconium-doped fungal biosorbents are represented in Table 6. All the four zirconium-doped fungal biosorbents followed the pseudo-second-order kinetic model with R^2 values > 0.99 as shown in Figure S2 and Table 6. This model is based on the assumption that in all the systems studied the chemical reaction seems to be the significant rate-controlling step. It is assumed that due to chemisorption the fluoride ions form covalent bonds by sharing or exchange of electrons with the biosorbent surface and hence fluoride removal takes place. The pseudo-second-order chemical reaction kinetics provides the best correlation of the experimental data over a long period [15].

As per the intraparticle diffusion model, the plot of uptake, q_t versus the square root of time ($t^{1/2}$) should be linear if intraparticle diffusion is the rate-controlling step for the adsorption process and if these lines pass through the origin [15]. If the plots do not pass through the origin, it is considered that some degree of boundary layer control influences the adsorption process. This also indicates that the intraparticle diffusion is not the only rate-limiting step, but other kinetic models may also control the rate of adsorption, all of which may be operating simultaneously. In the present study, all the four samples showed R^2 values greater than 0.975 and do not pass through the origin, which is an indication that both pseudo-second-order and intraparticle diffusion models best represent the biosorption kinetics.

3.4. Optimization of Process Variables. The optimum terms for adsorption of fluoride onto the surface of zirconium-doped fungal biomass were determined by means of the CCD under RSM. The equations representing the correlation

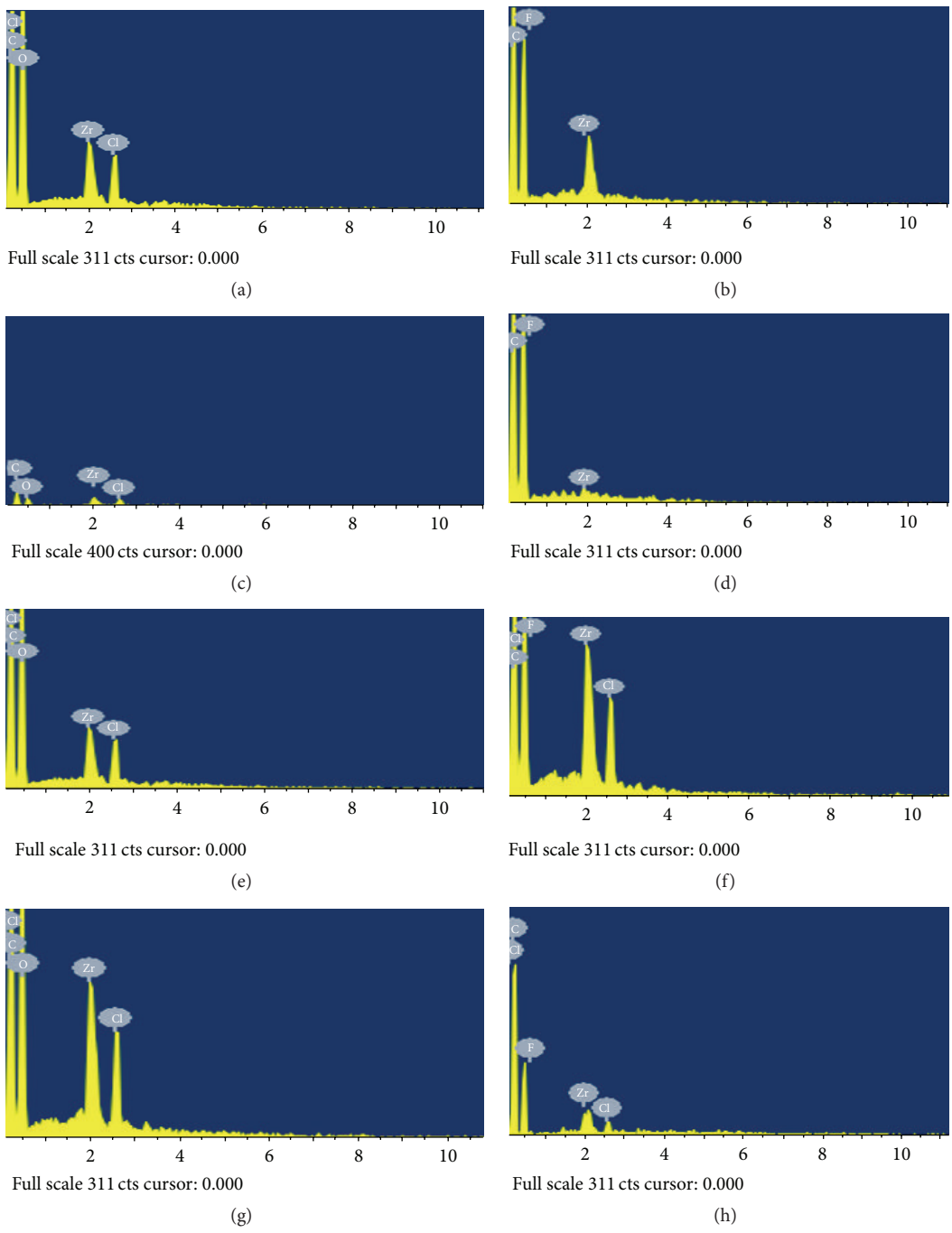

Figure 4: Chemical composition of zirconium-doped fungal biomass using EDS analysis: *Penicillium camemberti* SIT-CH-1 (a) before and (b) after adsorption, *Aspergillus ficuum* SIT-CH-2 (c) before and (d) after adsorption, *Aspergillus terreus* SIT-CH-3 (e) before and (f) after adsorption, and *Aspergillus flavipes* SIT-CH-4 (g) before and (h) after adsorption.

between the fluoride removal efficiency (Y) and the real values of the four influencing parameters, namely, pH, initial fluoride concentration, adsorbent dosage, and contact time, obtained by the application of RSM for the biomass of the four zirconium-doped fungi are represented in Table 7. The ANOVA results for the biomass of the four zirconium-doped fungi are presented in Tables S2–S5.

The state of the fitted model was declared by the coefficient of determination, R^2. The R^2 coefficient gives the relation of the total variation in the response predicted by the model. The values of R^2 closer to one indicate a strong relation between the experimental and the predicted results. This is also an indication that the model appropriately describes the association between the response and the parameters

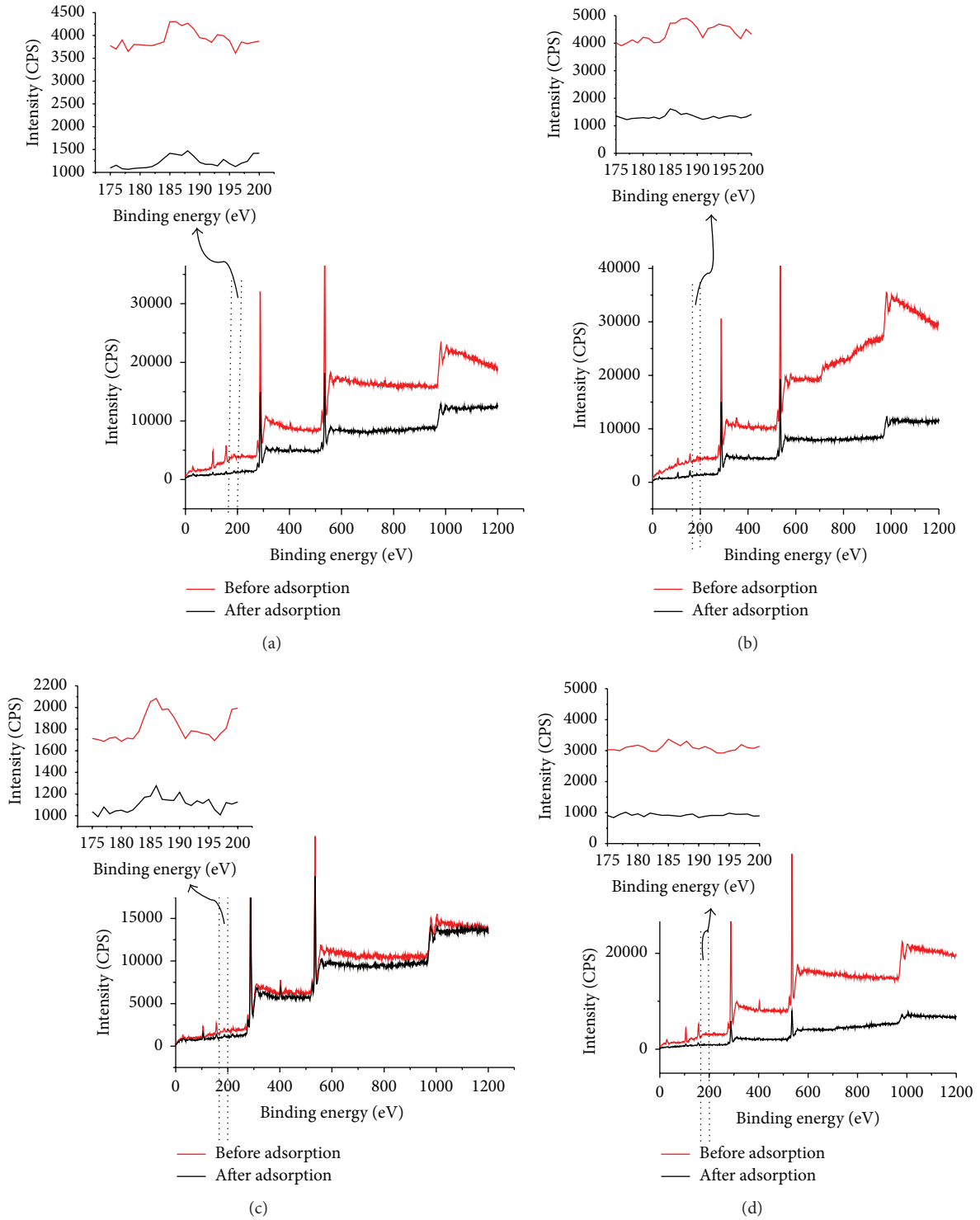

Figure 5: XPS plot of zirconium-doped (a) *Penicillium camemberti* SIT-CH-1, (b) *Aspergillus ficuum* SIT-CH-2, (c) *Aspergillus terreus* SIT-CH-3, and (d) *Aspergillus flavipes* SIT-CH-4 biomass before and after adsorption at pH 2. Inset: enlarged spectra with zirconium peak at 185 eV.

Table 6: Adsorption kinetic parameters for the fluoride removal by zirconium-doped fungal biosorbents.

Adsorption kinetic model	*Penicillium camemberti* SIT-CH-1 + zirconium	*Aspergillus ficuum* SIT-CH-2 + zirconium	*Aspergillus terreus* SIT-CH-3 + zirconium	*Aspergillus flavipes* SIT-CH-4 + zirconium
First-order model				
Rate constant, k_1 (min^{-1})	−0.569	1.52	3.47	0.83
Constants, q_1 (mg/g)	9.427	9.68	9.07	9.43
R^2	0.609	0.793	0.770	0.684
Pseudo-second-order model				
Rate constant, k_2 (g/mg·min)	−0.063	0.032	0.013	0.04
Constant, q_2 (mg/g)	9.284	9.893	9.616	9.609
R^2	0.999	0.999	0.998	0.999
Intraparticle diffusion model				
Rate constant, k_i ($mg/g{\cdot}min^{1/2}$)	−0.014	0.0811	0.165	0.0487
Constant, C	9.23	8.60	6.906	8.801
R^2	0.975	0.985	0.996	0.992
Elovich model				
Rate constant, α (mmole/g·min)	$-1.5E-70$	$3.22E10$	4641.886	$9.6E18$
Constant, β (g/mmole)	−0.057	0.342	0.68	0.19
R^2	0.891	0.976	0.961	0.928

Table 7: Correlation between fluoride removal efficiency (Y) and the four parameters in real values obtained by the application of RSM.

Species	Equation for percentage biosorption (Y) and the four test variables in real values
Penicillium camemberti SIT-CH-1 + zirconium	$Y = 105.01 - 0.127 * C_i - 4.289 *$ adsorbent dose $- 10.565 *$ pH $+ 0.003 *$ contact time $+ 0.167 * C_i$ $*$ adsorbent dose $+ 0.008 * C_i *$ pH $- 0.0004 * C_i *$ contact time $+ 6.124 *$ adsorbent dose $*$ pH $- 0.0009$ $*$ adsorbent dose $*$ contact time $+ 0.009 *$ pH $*$ contact time
Aspergillus ficuum SIT-CH-2 + zirconium	$Y = 62.17 + 0.067 * C_i + 75.47 *$ adsorbent dose $- 9.46 *$ pH $- 0.063 *$ contact time $+ 0.059 * C_i$ $*$ adsorbent dose $- 0.003 * C_i *$ pH $- 0.00014 * C_i *$ contact time $- 3.42 *$ adsorbent dose $*$ pH $+ 0.11$ $*$ adsorbent dose $*$ contact time $+ 0.022 *$ pH $*$ contact time $- 0.00071 * C_i^2 - 29.36 *$ adsorbent dose^2 $+ 0.096 *$ pH$^2 - 0.00018 *$ contact time^2
Aspergillus terreus SIT-CH-3 + zirconium	$Y = 91.71 - 0.00035 * C_i + 1.055 *$ adsorbent dose $- 10.16 *$ pH $+ 0.13 *$ contact time $- 0.00724 * C_i$ $*$ adsorbent dose $- 0.0013 * C_i *$ pH $- 0.00003 * C_i *$ contact time $+ 10.05 *$ adsorbent dose $*$ pH $+ 0.02 *$ adsorbent dose $*$ contact time $- 0.0076 *$ pH $*$ contact time $- 0.00002 * C_i^2 - 17.1$ $*$ adsorbent dose$^2 - 0.11 *$ pH$^2 - 0.00024 *$ contact time^2
Aspergillus flavipes SIT-CH-4 + zirconium	$Y = 122.46 - 0.28 * C_i - 23.45 *$ adsorbent dose $- 14.94 *$ pH $+ 0.043 *$ contact time $+ 0.17 * C_i$ $*$ adsorbent dose $+ 0.016 * C_i *$ pH $+ 0.00019 * C_i *$ contact time $+ 5.75 *$ adsorbent dose $*$ pH $- 0.019$ $*$ adsorbent dose $*$ contact time $- 0.005 *$ pH $*$ contact time $+ 0.0002 * C_i^2 + 14.34 *$ adsorbent dose^2 $+ 0.1 *$ pH$^2 - 0.000032 *$ contact time^2

[21]. Therefore, the proposed model could be used for future studies. The estimated effects and coefficients for the model are listed in Tables S2–S5. The model terms were evaluated by the p value (probability) with 99.99% confidence level. The p values were used to estimate whether F was large enough to indicate statistical significance and to check the significance of each coefficient. The p values lower than 0.0001 indicated that the model and the model terms were statistically significant.

3.4.1. Three Dimensional Response Surface Plots. The three dimensional response surface plots were used to investigate both main and interaction effects of the factors [21]. The response surface plots of the four zirconium-doped fungal species are represented in Supplementary Information (SI) file in Figures S3–S6. These plots indicate the percentage biosorption as a function of the four variables, that is, pH, initial fluoride concentration, biosorbent dosage, and contact time. The height of the surface represents the value of Y, the percentage biosorption.

3.4.2. Effect of Various Parameters. The behaviour of the biosorbent is mainly due to its cell wall structure and composition, which is considered to be the primary site of biosorption. The pH of the medium affects the ionization state of the functional groups on the biomass surface. Also, the zeta potential of the biomass is a function of pH. It can be observed that maximum F^- removal was at pH 2. As this pH is less than pH_{zpc}, the net charge on the surface of the biosorbents is positive due to the adsorption of excess hydrogen ion, which favors adsorption due to coulombic attraction. This is because the F^- ions, being negatively charged, have high affinity for positive charge on the biomass surface. The positive charge on the biomass increases with decreasing pH and is found to be maximum at pH 2. Hence, pH 2 was selected as the optimum for further experiments.

Table 8: Optimum conditions for biosorption of fluoride ions onto zirconium-doped fungal biomass.

Species	Initial concn./ppm	Ads. dose/g/L	pH	Contact time/min	Biosorption/%	Desirability
Penicillium camemberti SIT-CH-1 + zirconium	38	10.00	2.0	240	94.9	1.0
Aspergillus ficuum SIT-CH-2 + zirconium	100	10.00	2.0	134	95.98	1.0
Aspergillus terreus SIT-CH-3 + zirconium	100	7.45	2.0	240	95.2	1.0
Aspergillus flavipes SIT-CH-4 + zirconium	19	10.00	2.0	240	96.35	1.0

The percentage removal of the fluoride ions by adsorption onto the fungal biosorbents increased with increasing adsorbent dosage. Increase in the biosorbent dosage increases the surface area available for adsorption.

The effect of initial fluoride ion concentration in the aqueous solution on the extent of its removal was determined. The results indicate that the fluoride uptake increases with increasing initial fluoride concentration due to increasing driving force for mass transfer of F^- from aqueous solution to biosorbent surface. High concentrations of solute also help to overcome the overall mass transfer resistance leading to higher fluoride removal rates.

In a biosorption system, the contact time plays an important role, irrespective of the other experimental parameters affecting the biosorption kinetics. As the contact time increases, the percentage removal of the fluoride ions increases rapidly and after a certain time approaches an almost constant value indicating the attainment of an equilibrium condition at which the rate of adsorption of fluoride onto the surface of the sorbent is equal to the rate of desorption. This is attributable to the high driving force available initially, due to the high concentration of fluoride ions present. As the concentration of fluoride ions in solution decreases, the driving force for adsorption also decreases, leading to a lower adsorption rate.

Figure S7 illustrates that the data are well distributed near to a straight line, which indicates a good relationship between the experimental and predicted values of the response and the validity of the underlying assumptions.

3.5. Numerical Optimization. The fluoride ion adsorption process was optimized using numerical optimization and the optimum values of the various parameters are provided in Table 8. A desirability value of 1.0 was obtained after optimizing the process parameters.

3.6. Mechanism of Fluoride Removal. Fluoride removal by the fungal biosorbents appears to be due to the synergistic effect of electrostatic attraction, adsorption, and ion-exchange mechanisms. It has been demonstrated previously that fungi as well as algae are potential biosorbents for heavy metals [8, 22]. Fungi offer a wide range of chemical groups that can attract and sequester the fluoride ions in biomass. During adsorption, the fluoride ions mainly get deposited on the cell wall of the fungi [23]. The fungal cell wall is constituted of 90% polysaccharides, which include mainly glucans along with mannan, galactans, chitosan, or glycogen. While phosphate and carboxyl groups contribute negative charge to the cell wall, the amine groups of the chitosan produce a positive charge [24, 25]. The chitin or chitosan has lone pair of electrons on N or O groups and easily gets bound to hydrogen ions [25]. The negatively charged fluoride ions in turn get bound to H+ ions. But since the fungal cell wall contains only about 10% protein [24], the fluoride uptake by the amino acid functional groups is less. To increase the fluoride adsorption, the fungal species are doped with tetravalent zirconium. Zirconium bonds strongly with negatively charged groups present on the fungal cell wall and also has high affinity towards fluoride ions.

The type of fungal species, biosorbent dosage, and solution pH also seem to influence the uptake capacity [26, 27]. Similar findings have been obtained for the biosorption of uranium, copper, and humic acids [28]. The weak shifts of the functional amide peak observed in the FTIR analysis (Figure 1) indicated that the fluoride species biosorption involves electrostatic attraction. In fluoride solution, the fluoride ions get adsorbed onto the sorbent surface. In acidic medium, where the concentration of H^+ ions is high, the sorbent surface acquires a net positive charge which in turn attracts more fluoride ions and forms hydrogen bonds and hence there is a significant increase in fluoride removal at lower pH [29]. As the pH increases, the surface slowly acquires a net negative charge, which repels fluoride ions and hence fluoride removal by electrostatic attraction is ruled out in alkaline medium. In addition to electrostatic attraction, the removal of fluoride may also be controlled by ion exchange with negative ions such as hydroxyl, carboxyl, and chloride ions present on the doped biosorbent [30].

4. Conclusions

From the above studies, it appears that fluoride removal is due to adsorption, electrostatic attraction, and ion exchange. It was found that the zirconium-doped biosorbent could remove fluoride ions at higher as well as lower concentrations. The present study was conducted using clean water spiked with different concentrations of fluoride. For treating industrial wastewater with a highly complex composition, further tests should be done to confirm its usage for treating high concentration effluents. The conditions at which maximum fluoride removal takes place were optimized by using CCD of RSM. It was shown that the simultaneous optimization of the multiresponse system by desirability function indicated that greater than 94% adsorption of fluoride was possible by using the optimal conditions of the four parameters for the four fungal species studied. The adsorption equilibrium data were in good agreement with the Langmuir and Freundlich isotherms. The kinetics of fluoride adsorption could be best described by the pseudo-second-order kinetic model for all the tested adsorbents. The biosorbent can be further used

to treat large quantities of water by immobilizing it onto a suitable matrix and using it as a packing material in fixed-bed. The biosorbent can also be regenerated and reused.

Competing Interests

The authors declare that there is no conflict of interests regarding the publication of this paper.

Acknowledgments

The authors would like to thank the Director, Principal, and Management of Siddaganga Institute of Technology, Tumkur, for their support.

References

[1] D. L. Ozsvath, *Reviews in Environmental Science and Biotechnology*, 2009.

[2] WHO, "Guidelines for drinking water quality," in *Health Criteria and Other Supporting Information*, vol. 2, World Health Organization, Geneva, Switzerland, 2nd edition, 1984.

[3] BIS (Bureau of Indian Standards), "Indian standard specifications for drinking water," Tech. Rep. IS:10500, 1992.

[4] RGNDWM, *Prevention and Control of Fluorosis in India, Water Quality and Defluoridation Techniques*, vol. 11, Rajiv Gandhi National drinking Water Mission, Ministry of Rural Development, New Delhi, India, 1993.

[5] M. G. García and L. Borgnino, "Fluoride in the context of the environment," *Fluorine: Chemistry, Analysis, Function and Effects*, vol. 3, chapter 1, 2015.

[6] C. R. Nagendra Rao, "Fluoride and environment—a review," in *Proceedings of the 3rd International Conference on Environment and Health*, M. J. Bunch, V. M. Suresh, and T. V. Kumaran, Eds., Chennai, India, December 2003.

[7] J. Singh, P. Singh, and A. Singh, "Fluoride ions vs removal technologies: a study," *Arabian Journal of Chemistry*, 2014.

[8] B. Volesky and Z. R. Holan, "Biosorption of heavy metals," *Biotechnology Progress*, vol. 11, no. 3, pp. 235–250, 1995.

[9] M. Rajan and G. Alagumuthu, "Study of fluoride affinity by zirconium impregnated walnut shell carbon in aqueous phase: kinetic and isotherm evaluation," *Journal of Chemistry*, vol. 2013, Article ID 235048, 8 pages, 2013.

[10] S. Ray, "RSM: a statistical tool for process optimization," *Indian Textile Journal*, vol. 117, pp. 24–30, 2006.

[11] G. Derringer and R. Suich, "Simultaneous optimization of several response variables," *Journal of Quality Technology*, vol. 12, no. 4, pp. 214–219, 1980.

[12] I. A. W. Tan, A. L. Ahmad, and B. H. Hameed, "Adsorption of basic dye on high-surface-area activated carbon prepared from coconut husk: equilibrium, kinetic and thermodynamic studies," *Journal of Hazardous Materials*, vol. 154, no. 1–3, pp. 337–346, 2008.

[13] B. Malgorzata, "Adsorption on heterogeneous surfaces," in *Adsorption: Theory, Modeling and Analysis*, J. Tóth, Ed., pp. 112–115, CRC Press, New York, NY, USA, 2002.

[14] H. Chhipa, R. Acharya, M. Bhatnagar, and A. Bhatnagar, "Determination of sorption potential of fermentation industry waste for fluoride removal," *International Journal of Bioassays*, vol. 2, no. 3, pp. 568–574, 2013.

[15] S. V. Mohan, S. V. Ramanaiah, and P. N. Sarma, "Biosorption of direct azo dye from aqueous phase onto *Spirogyra* sp. I02: evaluation of kinetics and mechanistic aspects," *Biochemical Engineering Journal*, vol. 38, no. 1, pp. 61–69, 2008.

[16] X. Dou, D. Mohan, C. U. Pittman, and S. Yang, "Remediating fluoride from water using hydrous zirconium oxide," *Chemical Engineering Journal*, vol. 198-199, pp. 236–245, 2012.

[17] B. C. Smith, *Infrared Spectral Interpretation: A Systematic Approach*, CRC Press, London, UK, 1st edition, 1998.

[18] F. Amin, F. N. Talpur, A. Balouch, M. A. Surhio, and M. A. Bhutto, "Biosorption of fluoride from aqueous solution by white-rot fungus *Pleurotus eryngii* ATCC 90888," *Environmental Nanotechnology, Monitoring & Management*, vol. 3, pp. 30–37, 2015.

[19] S. K. Shakshooki, B. Mohamed Hassan, K. W. EL-Nowely, A. El-Belazi, S. M. Abed, and M. M. Al-Said, "α-zirconium titanium phosphates-fibrous cerium phosphate composite membranes and their 1,10- Phenanthroline Cu(II) pillared materials," *Physics and Materials Chemistry*, vol. 2, no. 1, pp. 7–13, 2014.

[20] T. Tanuma, H. Okamoto, K. Ohnishi, S. Morikawa, and T. Suzuki, "Activated zirconium oxide catalysts to synthesize dichloropentafluoropropane by the reaction of dichlorofluoromethane with tetrafluoroethylene," *Applied Catalysis A: General*, vol. 359, no. 1-2, pp. 158–164, 2009.

[21] U. K. Garg, M. P. Kaur, V. K. Garg, and D. Sud, "Removal of Nickel(II) from aqueous solution by adsorption on agricultural waste biomass using a response surface methodological approach," *Bioresource Technology*, vol. 99, no. 5, pp. 1325–1331, 2008.

[22] J. L. Zhou, "Zn biosorption by *Rhizopus arrhizus* and other fungi," *Applied Microbiology and Biotechnology*, vol. 51, no. 5, pp. 686–693, 1999.

[23] B. Volesky, "Biosorption by fungal biomass," in *Biosorption of Heavy Metals*, B. Volesky, Ed., p. 139, CRC Press, Boca Raton, Fla, USA, 1990.

[24] J. Remacle, "The cell wall and metal binding," in *Biosorption of Heavy Metals*, B. Volesky, Ed., p. 82, CRC Press, Boca Raton, Fla, USA, 1990.

[25] G. Naja, C. Mustin, B. Volesky, and J. Berthelin, "A high-resolution titrator: a new approach to studying binding sites of microbial biosorbents," *Water Research*, vol. 39, no. 4, pp. 579–588, 2005.

[26] F. Veglio' and F. Beolchini, "Removal of metals by biosorption: a review," *Hydrometallurgy*, vol. 44, no. 3, pp. 301–316, 1997.

[27] G. M. Gadd, C. White, and L. De Rome, "Heavy metal and radionuclide uptake by fungi and yeasts," in *Biohydrometallurgy*, P. R. Norris and D. P. Kelly, Eds., A. Rowe, Chippenham, UK, 1988.

[28] H. Niu and B. Volesky, "Biosorption of anionic metal complexes," in *Biohydrometallurgy: Fundamentals, Technology and Sustainable Development, Part B—Biosorption and Bioremediation*, V. S. T. Ciminelli and J. O. Garcia, Eds., p. 189, Elsevier Science B.V., Amsterdam, The Netherlands, 2001.

[29] G. Naja and B. Volesky, "The mechanism of metal cation and anion biosorption," in *Microbial Biosorption of Metals*, P. Kotrba, M. Mackova, and T. Macek, Eds., pp. 19–58, Springer, Dordrecht, The Netherlands, 2011.

[30] G. A. F. Roberts, *Chitin Chemistry*, Macmillan, London, UK, 1992.